Ecological Indicators 94 (2018) 292–304

Contents lists available at ScienceDirect

Ecological Indicators

journal homepage: www.elsevier.com/locate/ecolind

Spatio-temporal variations in water use efficiency and its drivers in China over the last three decades

Shaobo Sun[a], Zhaoliang Song[a,*], Xiuchen Wu[b,c], Tiejun Wang[a], Yuntao Wu[a], Wenli Du[a], Tao Che[d,e], Chunlin Huang[d,e], Xuejun Zhang[f], Bo Ping[a], Xiaofeng Lin[e,g], Pan Li[e,h], Yaoxian Yang[e,i], Baozhang Chen[e,g,*]

[a] Institute of Surface-Earth System Science, Tianjin University, Tianjin 300072, China
[b] State Key Laboratory of Earth Surface Processes and Resource Ecology, Beijing Normal University, Beijing 100875, China
[c] Faculty of Geographical Science, Beijing Normal University, Beijing 100875, China
[d] Heihe Remote Sensing Experimental Research Station, Northwest Institute of Eco-Environment and Resources, Chinese Academy of Sciences, Lanzhou 730000, China
[e] University of Chinese Academy of Sciences, Beijing 100049, China
[f] Key Laboratory of Water Cycle and Related Land Surface Processes, Institute of Geographical Sciences and Natural Resources Research, Chinese Academy of Sciences, Beijing 100101, China
[g] State Key Laboratory of Resources and Environment Information System, Institute of Geographic Sciences and Natural Resources Research, Chinese Academy of Sciences, Beijing 100101, China
[h] State Key Laboratory of Environmental Geochemistry, Institute of Geochemistry, Chinese Academy of Sciences, Guiyang 550081, China
[i] State Key Laboratory of Numerical Modeling for Atmospheric Sciences and Geophysical Fluid Dynamics, Institute of Atmospheric Physics, Chinese Academy of Sciences, Beijing 100029, China

ARTICLE INFO

Keywords:
Water use efficiency (WUE)
Process-based model
Gross primary productivity (GPP)
Evapotranspiration (ET)
Inter-annual variation

ABSTRACT

Ecosystem water use efficiency (WUE) reflects the intimately coupled relationship between the carbon and water cycles in terrestrial ecosystems. However, the inter-annual variation and its drivers of WUE are poorly understood at regional/global scale, due to either limited data availability or uncertainties in current data streams. In this study, we used process-based models simulated gross primary productivity (GPP) and evapotranspiration (ET) data to estimate the ecosystem WUE (eWUE, GPP/ET) in China for 1979–2012. The eWUE estimates were validated against eddy covariance-based values from 35 flux towers. The inter-annual variation of the eWUE was quantified and its responses to annual precipitation (AP), annual mean temperature (AMT), and annual mean leaf area index (AMLAI) were analyzed. The key findings were as follows. (i) The mean annual eWUE over China was $1.48 \pm 1.04\,g\,C\,kg^{-1}\,H_2O$ and had a slightly increasing but not significant trend ($7.32 \times 10^{-4}\,g\,C\,kg^{-1}\,H_2O\,yr^{-1}$, $p < 0.05$) from 1979 to 2012. (ii) The spatial distribution of the eWUE trend showed large spatial variability. ~21.4% and ~19.0% of vegetated land in China had significant increasing and decreasing trends (Mann-Kendall test, $p < 0.1$), respectively. The increasing eWUE was mainly found in the northeast, southwest, and central areas of China, while the decreasing eWUE was mostly distributed in west China. (iii) The inter-annual variation of the spatially averaged annual eWUE was negatively correlated with that of AP and AMT, and positively correlated with that of AMLAI. In ~41.4%, ~9.9%, and ~3.1% of vegetated land in China the inter-annual variation of eWUE was dominated by the inter-annual variations of AP, AMT, and AMLAI, respectively. In most land of north China and west China the inter-annual variation of eWUE was dominated by the inter-annual variation of AP, while in central, east and south China all the AP, AMT, AMLAI, and other drivers played important roles.

1. Introduction

Water use efficiency (WUE) is a key parameter that reflects the integrated effects of the water, energy, and carbon cycles on ecosystem processes (Ito and Inatomi, 2012; Keenan et al., 2013). Therefore, quantifying the spatio-temporal variations in WUE and revealing its drivers are crucial to understand both the patterns in terrestrial ecosystem carbon-water coupling and their responses to climate change. This provides insight into regional vegetation growth prediction and ecosystem management (Liu et al., 2016; Cheng et al., 2017; Huang

* Corresponding authors at: No. 92 Weijin Road, Nankai District, Tianjin 300072, China (Z. Song). 11A, Datun Road, Chaoyang District, Beijing, 100101, China (B. Chen).
E-mail addresses: zhaoliang.song@tju.edu.cn (Z. Song), baozhang.chen@igsnrr.ac.cn (B. Chen).

https://doi.org/10.1016/j.ecolind.2018.07.003
Received 11 April 2018; Received in revised form 30 June 2018; Accepted 2 July 2018
1470-160X/

et al., 2016; Knauer et al., 2017).

The definition of WUE varies at different level of organizations (Ponton et al., 2006; Beer et al., 2009; Zhou et al., 2014; Boese et al., 2017). At the ecosystem scale, a widely used WUE indicator (eWUE) is the ratio of gross primary productivity (GPP) to evapotranspiration (ET) (Reichstein et al., 2007; Huang et al., 2015; Guerrieri et al., 2016). It represents the adjustment of vegetation photosynthesis to water loss (Huang et al., 2015). In recent decades, many studies have investigated the spatio-temporal patterns in eWUE across a wide range of ecosystems by using ET and GPP from eddy covariance (EC) observations (Hu et al., 2008; Yu et al., 2008; Bruemmer et al., 2012; Zhu et al., 2015; Guerrieri et al., 2016; Xie et al., 2016; Jones et al., 2017), satellite remote sensing (Lu and Zhuang, 2010; Tang et al., 2014; Gang et al., 2016; Huang et al., 2017; Yu et al., 2017), and process-based land models (e.g., terrestrial ecosystem model [TEM] or land surface model [LSMs]) (Tian et al., 2011; Huang et al., 2015; Sun et al., 2016a). Nevertheless, it is still difficult to accurately quantify eWUE at regional and global scales, because of the difficulties in the estimation of reliable GPP and ET data (Zhang et al., 2015a, 2016; Oliveira et al., 2017; Tang et al., 2017). To well estimate regional and global eWUE, it is critical to first obtain reliable ET and GPP datasets.

Because eWUE not only depends on the strength of the coupling strength between GPP and ET but also on its responses to climatic and biotic factors (Huang et al., 2016), the spatio-temporal variations of eWUE can be quite obvious and its drivers vary with ecosystem types and spatial scales. Many studies have reported the eWUE variations and its drivers at site scale (Hu et al., 2008; Yu et al., 2008; Xiao et al., 2013; Zhu et al., 2015; Helman et al., 2017; Quan et al., 2018). However, our knowledge about the eWUE variations and its drivers at regional and global scales is still uncomplete, because the regional and global eWUE estimates are always associated with significant uncertainties and the control factors of eWUE are largely varied with ecosystem types. For example, based on remote sensing GPP and ET data, Tang et al. (2014) estimated global eWUE and found a negative eWUE trend with a value of -4.5×10^{-3} g C kg^{-1} H_2O yr^{-1} over 2000–2013. On contrary, Xue et al. (2015) and Cheng et al. (2017) both reported significant and positive global eWUE trends during the same period, based on remote sensing and process-based model methods, respectively. In addition, based on EC-derived eWUE, Yu et al. (2008) reported that annual eWUE linearly decreased with annual precipitation (AP) and annual mean temperature (AMT). In comparison, using measurements from more EC sites, Zhu et al. (2015) found that the eWUE changed with AP in a logarithmical manner and linearly increased with AMT. At global, Xue et al. (2015) found that in most land areas, eWUE was positively correlated with AP and negatively correlated with AMT, respectively.

China has an enormous land area, encompassing a large range of ecosystems and climate types. The extreme diversity in climate, ecozones, land cover, soil, and topography leads to a considerable spatio-temporal variability in eWUE and makes it difficult to accurately estimate eWUE at the national scale. Recently, Liu et al. (2015) and Zhang et al. (2015a) estimated eWUE in China using process-based model and remote sensing approaches, respectively. However, the periods studied were limited to after 2000, and the controls on the spatio-temporal variations in eWUE and the uncertainties associated with the eWUE estimates were not fully discussed.

Process-based models forced with observation-based inputs provide relatively ideal tools to estimate eWUE and investigate its responses to drivers at site- to global scale, and have the advantage of explicitly including main physiological processes that control eWUE over long time periods (Tian et al., 2011; Huang et al., 2015). Here, using GPP and ET data from process-based land surface models, we estimate the eWUE and analyze it main drivers across China. The three main objectives were to (i) estimate annual eWUE in China over the last three decades (i.e., 1979–2012), (ii) quantify the spatio-temporal variations in eWUE over China during the last three decades, and (iii) examine the response of the inter-annual variation of eWUE to that of the climatic (e.g., precipitation and temperature) and biotic (e.g., leaf area index [LAI]) variables.

2. Materials and methods

2.1. ET and GPP data

In our previous work, based on multiple LSMs simulations we have developed a China ET dataset (Hereafter LSMs-ET), which has a spatial resolution of 0.25° × 0.25° and covers the period 1979–2012 (Sun et al., 2017). This ET data was used to estimate eWUE over China in this study. It has been evaluated against measurements from nine EC towers and ET estimates derived from regional water-balance analyses. In addition, it was also compared with independent ET products from remote sensing (Mu et al., 2007) and upscaling (Jung et al., 2011) methods. More details of the ET dataset can be found in Sun et al. (2017).

The GPP data used in this study were generated by forcing a

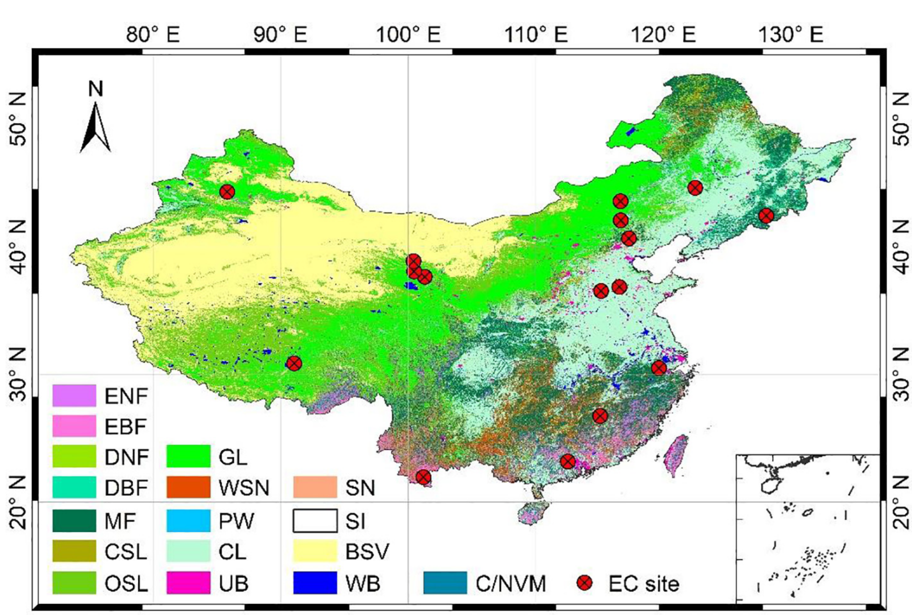

Fig. 1. Location of the EC-GPP flux tower sites used in this study. The base map is MODIS land-cover product for 2001 (Friedl et al., 2002). The land cover types include evergreen needleleaf forests (ENF), evergreen broadleaf forests (EBF), deciduous needleleaf forests (DNF), deciduous broadleaf forests (DBF), mixed forests (MF), closed shrublands (CSL), open shrublands (OSL), grasslands (GL), woody savannas (WSN), permanent wetlands (PW), croplands (CL), urban and built-up lands (UB), savannas (SN), snow and ice (SI), barren or sparsely vegetated lands (BSV), water bodies (WB), and cropland/natural vegetation mosaics (C/NVM).

process-based model with observation-based meteorological forcing and soil datasets. It has the same spatio-temporal resolution and time period as the LSMs-ET data. Before it was used to estimate eWUE, the GPP data was first validated against the EC-derived GPP from 16 China flux towers and then compared with independent GPP products from remote sensing and upscaling methods. The details of the model and the GPP simulations are provided in the following sections.

2.2. EC flux tower data

The EC data used in this study included two datasets. The first was the EC-derived GPP data (EC-GPP), which was used to validate our process-based model GPP simulations in this study. It included measurements from 16 EC flux towers and were collected from published papers and the Chinese flux observation and research network (ChinaFlux, Yu et al., 2006). The second was the EC-based eWUE data (EC-eWUE), which were extracted from Liu et al. (2015) and included 35 flux towers. It should be noted that some of the flux towers used in the two EC datasets were same.

The land cover types of the EC-GPP sites included six croplands, five grasslands, two mixed forests, two evergreen broadleaf forests, and a woody savanna (Fig. 1). For the sites that did not directly provided GPP estimates, we used the REddyProcWeb online tool (https://www.bgc-jena.mpg.de/bgi/index.php/Services/REddyProcWeb) to fill data gaps and partition the net ecosystem exchange of CO_2 (NEE) into GPP and ecosystem respiration (R_e). A total of 39 site-year EC-derived GPP measurements were collected (Table 1).

The land cover types of the 35 EC-eWUE sites consisted of 13 forests, 14 grasslands, five croplands, and three wetlands, across a range of climate zones (Fig. S1). For each site the annual eWUE during the observing periods was provided (Table S1). More details about this EC-eWUE dataset can be found in Liu et al. (2015).

Supplementary data associated with this article can be found, in the online version, at https://doi.org/10.1016/j.ecolind.2018.07.003.

2.3. The models

We used the Dynamic Land Model (DLM) to estimate GPP in China over 1979–2012. DLM is the recently updated version of the Ecosystem-Atmosphere Simulation Scheme (EASS), which is a remote sensing-based LSM developed by Chen et al. (2007a, 2007b). The current DLM has been coupled to the Community Land Model, version 4.0 (CLM4.0) framework (Oleson et al., 2010) by replacing the original photosynthesis and energy flux modules with the EASS based formulations and optimizing the parameters (Chen et al., 2013). Recently, the DLM model has been improved by adding a vegetation dynamic model with a state-of-art phenology module (Chen and Che, 2016) and modifying soil moisture and temperature parameterizations (Sun et al., 2016b). The validations showed that the improved model performs well in radiation, evapotranspiration, gross primary production (GPP) simulations (Chen et al., 2013; Yan et al., 2014; Sun et al., 2017).

In this study, the DLM model was run offline from 1979 to 2012 at a spatial resolution and time step of 0.25° × 0.25° and daily, respectively. Before obtaining the GPP outputs, the model was spun-up for 34 years (from 1979 to 2012). The photosynthesis parameters in the DLM model for different plant functional types were the optimized ones from Chen et al. (2013) (Table S2).

2.4. Model inputs

Instead of using the reanalysis-based forcing that is taken as a default by the models, we adopted an observation-based China high resolution meteorological forcing dataset to drive the DLM model. The forcing dataset was produced by the Data Assimilation and Modeling Center for Tibetan Multi-spheres, Institute of Tibetan Plateau Research, Chinese Academy of Sciences (Yang et al., 2010). It covers the period from 1979 to 2012, with a temporal resolution of 3 h and spatial resolution of 0.1° × 0.1°. It was produced by merging observations from 740 meteorological stations operated by the China Meteorological Administration, the Global Land Data Assimilation System dataset, and several satellite remotely sensed meteorological products.

For the land surface datasets, we used a recently developed soil texture dataset with a 30 arc-second resolution to replace the model defaults. The dataset was developed for LSMs at Beijing Normal University (Shangguan et al., 2013). It was produced by merging soil information from 8979 soil profiles and the Soil Map of China. The LAI data was prescribed Moderate Resolution Imaging Spectroradiometer (MODIS) derived LAI. Other model land surface datasets were taken from the model defaults, which were derived from satellite remote sensing or synthetic land surface characteristic products.

2.5. Climate, satellite and other auxiliary data

We considered precipitation and temperature as the climatic drivers and LAI as the biotic driver that mostly contribute to eWUE variations. The precipitation and temperature data used were downloaded from the China Meteorological Data Service Center (http://data.cma.cn/en). They were produced by interpolating observations from 2472 China meteorological stations from 1961 onwards at monthly time scales and a spatial resolution of 0.5° × 0.5°. To match our eWUE estimates, they were regridded to a spatial resolution of 0.25° × 0.25° and then aggregated to annual values.

The LAI data were retrieved from the Global Inventory Modeling and Mapping Studies third generation (GIMMS3g) LAI product, which

Table 1
Characteristics of the EC-GPP flux tower sites.

Sites	Coordinates	IGBP classes	Start-end years	References
CN-Cha	42.40°N, 128.10°E	Mixed Forests	2003–2005	ChinaFlux
CN-Yuc	36.95°N, 116.60°E	Croplands (maize)	2003–2005	ChinaFlux
CN-Xsh	21.95°N, 101.20°E	Evergreen Broadleaf Forests	2003–2005	ChinaFlux
CN-Qia	26.73°N, 115.07°E	Woody Savannas	2003–2005	ChinaFlux
CN-Din	23.17°N, 112.53°E	Evergreen Broadleaf Forests	2003–2005	ChinaFlux
CN-Hab	37.61°N, 101.31°E	Grasslands	2003–2005	ChinaFlux
CN-Dan	30.85°N, 91.08°E	Grasslands	2004–2005	ChinaFlux
CN-Nmg	43.55°N, 116.68°E	Grasslands	2003–2005	ChinaFlux
CN-Du1	42.05°N, 116.67°E	Croplands	2005–2006	Li et al. (2013)
Miyun	40.63°N, 117.32°E	Croplands (fruiter)	2008–2010	Liu et al. (2013)
Tongyu	44.59°N, 122.52°E	Grasslands	2004–2006	Wang et al. (2010)
Guantao	36.52°N, 115.13 °E	Croplands (maize)	2009–2010	Liu et al. (2013)
Wulws	36.52°N, 115.13 °E	Cropland (cotton)	2009–2010	Wang et al. (2015)
Yingke	38.85°N, 100.42 °E	Croplands (maize)	2008–2009	Liu et al. (2008)
Arou	38.05°N, 100.46°E	Grasslands	2010	Ma et al. (2008)
Anji	30.48°N, 119.67°E	Mixed Foresrs	2011	Zhang and Ge (2014)

was derived from the GIMMS3g normalized difference vegetation index (NDVI) product using a neural network algorithm. It covers period of 1981–2011 and has a spatial and temporal resolution of 1/12° and bi-monthly, respectively. More details about the GIMMS3g LAI product can be found in Zhu et al. (2013).

Several auxiliary datasets were used to further evaluate and analyze our GPP and eWUE estimates, including the MODIS GPP (MOD17 version 055, Zhao and Running, 2010), the model tree ensemble (MTE)-based upscaled GPP (MTE-GPP, Jung et al., 2011), the MODIS land-cover (Friedl et al., 2002), and the GIMMS3g NDVI data (Tucker et al., 2005). The MOD17 GPP was derived from NASA Earth Observing System satellite data since 2000 and provides GPP estimates at 1-km spatial resolution and 8-day intervals. In this study, the monthly MOD17 GPP was used and aggregated to a spatial resolution of 0.25° × 0.25°. The MTE-GPP was an observation-driven global monthly gridded GPP. It was produced by first training the MTEs based on remote sensing indices, climate and meteorological data, and land use information at site-level and then applying the MTEs to generate global GPP with a 0.5° × 0.5° spatial resolution and a monthly temporal resolution. The MTE-GPP was regridded to a spatial resolution of 0.25° × 0.25° before it was used to evaluate our modeled GPP. The MODIS 1 km land cover data in 2001 were used to analyze eWUE variations among the main vegetation types. The GIMMS3g NDVI were used to extract out the vegetated land in China by identifying the pixels with maximum NDVI values larger than 0.1.

2.6. Methods

We used the linear least-square regression method to determine the spatially averaged eWUE trends. An F test was used to examine the statistical significance of the trends, and a p value < 0.05 was considered significant. A breakpoint (BP) detecting method as described in Chen et al. (2014) was used to further determine the eWUE variation, with significant slope values ($p < 0.05$).

The nonparametric Mann-Kendall (M-K) test (Mann, 1945; Kendall, 1975) method was used to determine annual eWUE trends and to quantify the statistical significance of the trends for each pixel. According to the Z-values from the M-K test, the eWUE pixels were divided into seven classes: significant decrease (Z-value < -2.32, with $p < 0.01$); medium decrease (Z-value < -1.96, with $p < 0.05$); decrease (Z-value < -1.65, with $p < 0.1$); not significant ($|$Z-value$| < -1.65$); increase (Z-value > 1.65, with $p < 0.1$); medium increase (Z-value > 1.96, with $p < 0.05$); and significant increase (Z-value > 2.32, with $p < 0.01$).

The multiple linear regression approach was used to diagnose the responses of the inter-annual variation of the spatially averaged eWUE to that of the drivers over China:

$$y = \gamma_{\mathrm{pre}} \times P + \delta_{\mathrm{tem}} \times T + \varphi_{\mathrm{lai}} \times LAI + \varepsilon \tag{1}$$

where y is the spatially averaged annual eWUE; P, T, and LAI are the spatially averaged AP, AMT, and annual mean leaf area index (AMLAI), respectively. All the variables, including y were normalized values (Eq. (2)).γ_{pre}, δ_{tem}, and φ_{lai} are the fitted regression coefficients. ε is the residual error term. As described in Piao et al. (2013), although γ_{pre}, δ_{tem}, and φ_{lai} are not the true sensitivities of eWUE to the derivers, they can be regarded as apparent sensitivities and used to represent the contributions of variations in each driver to the eWUE variation.

$$z_i = \frac{x_{\mathrm{i}} - \bar{x}}{\sigma} \tag{2}$$

where x_i is the eWUE or driver variables in ith year. $\bar{x}$ and σ are the mean and the standard deviation of variable x, respectively. z_i is the normalized x in ith year.

To quantify the relative contributions of the inter-annual variation of each driver to eWUE for each pixel, we also performed partial correlation analysis between eWUE and one driver after statistically

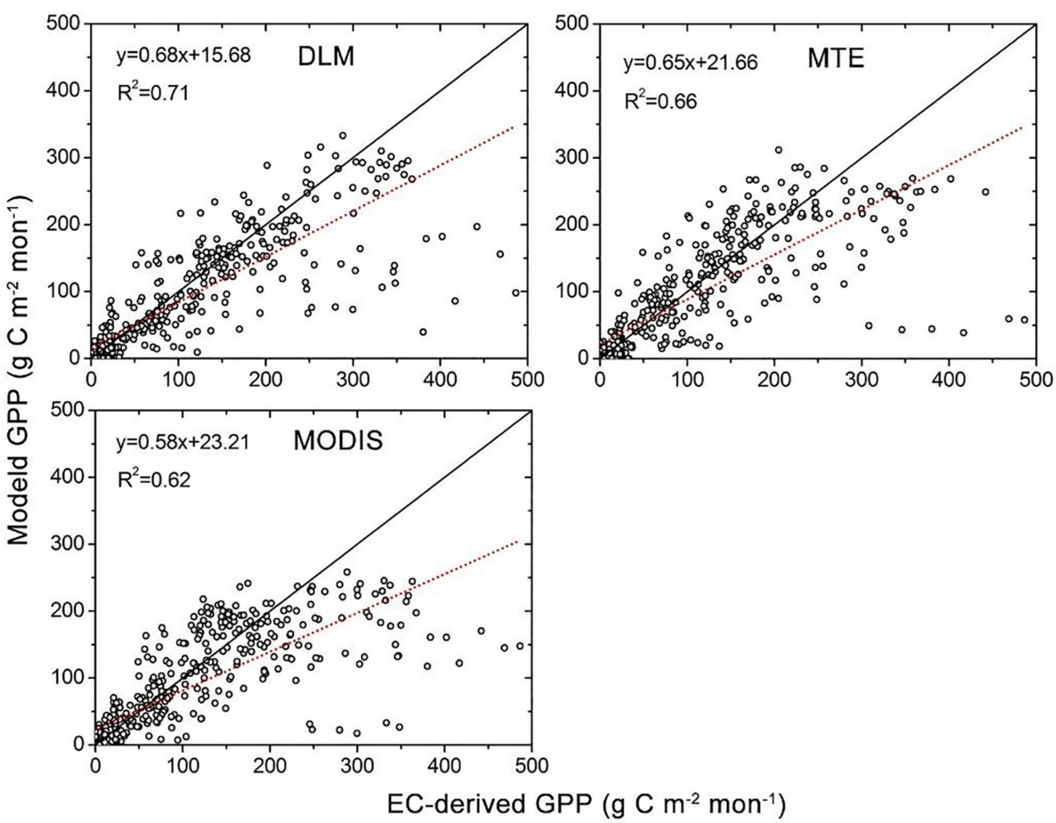

Fig. 2. The GPP datasets vs. monthly GPP values from 16 EC sites (Table 1). The solid and dashed lines are the 1:1 and regression lines, respectively. The values of DLM, MODIS, and MTE GPP were from grids that encompass the tower locations.

controlling changes in the other drivers. For example, the partial correlation coefficient between eWUE and AP ($r_{eWUE-P,(T,LAI)}$) was calculated as following:

$$r_{eWUE-P,(T,LAI)} = \frac{r_{eWUE-P,(T)} - r_{eWUE-LAI,(T)} * r_{P-LAI,(T)}}{\sqrt{(1 - r_{eWUE-LAI,(T)}{}^2) * (1 - r_{P-LAI,(T)}{}^2)}} \tag{3}$$

where $r_{eWUE-P,(T)}$ is the partial correlation coefficient between eWUE and AP after statistically controlling the AMT:

$$r_{eWUE-P,(T)} = \frac{r_{eWUE-P} - r_{eWUE-T} * r_{P-T}}{\sqrt{(1 - r_{eWUE-T}{}^2) * (1 - r_{P-T}{}^2)}} \tag{4}$$

where r_{eWUE-P}, r_{eWUE-T}, and r_{P-T} is the simple correlation coefficients for eWUE-AP, eWUE – AMT, and AP-AMT, respectively. $r_{eWUE-LAI,(T)}$ and $r_{P-LAI,(T)}$ in Eq. (3) were analogous to $r_{eWUE-P,(T)}$.

Following Wang et al. (2017), based on the partial correlation coefficients between the drivers and eWUE, we also constructed a map of eWUE dominant drivers to reveal the spatial variability of eWUE dominant driver over China.

3. Results

3.1. GPP evaluations

Before estimating the eWUE, we first estimated the GPP of China for 1979–2012 using the DLM model. The GPP estimate were validated against EC-derived values from 16 flux towers and independent estimates from MODIS and MTE GPP. The EC-based evaluations showed that our DLM GPP had the highest coefficient of determination (R^2), with a value of 0.71, followed by the MTE and MODIS GPP, with R^2 values of 0.66 and 0.62, respectively (Fig. 2). Nevertheless, as with the MTE and MODIS GPP, overall the DLM GPP also underestimated the measurements. Comparisons between these three GPP datasets and EC observations at each site suggested that the GPP underestimations occurred mainly at arid and semi-arid crop sites (Fig. S2, Wulws and Yingke) during growing seasons. This result was consistent with previous studies that the uncertainties of GPP estimates from current process-based models are high for heavily managed agricultural areas (Guanter et al., 2014). Moreover, our DLM GPP estimated a mean annual GPP of 5.66 Pg C over China (2000–2011), which was intermediate between that of MODIS (5.16 Pg C) and MTE (6.52 Pg C) GPP. The spatial patterns of the mean annual GPP of DLM, MODIS, and MTE were also similar. Overall, our evaluation validated the reliability of the DLM GPP dataset, and thus it can be used to further estimate the eWUE over China.

3.2. eWUE evaluations

Based on the DLM GPP and the LSMs-ET, we estimated the eWUE in China for 1979–2012. We used the EC-eWUE data from Liu et al. (2015) (Table S1 & Fig. S1) to validate our eWUE estimates. The validations showed that our eWUE estimates explained 64% of the EC-eWUE variability (Fig. 3), with a mean bias (*BIAS*) and root-mean-square error (*RMSE*) value of −0.19 and 0.58 g C kg^{-1} H_2O, respectively. It was not surprised that the cropland sites had large uncertainties, especially at the Yinke site, due to the significant uncertainties in the GPP simulations at those sites. The annual eWUE estimates for grassland sites ranged from 0.37 to 1.43 g C kg^{-1} H_2O, which had the best agreement with EC-eWUE, when compared to the other land cover types. Except for the Kubuqi site, the annual eWUE estimates of forest sites were higher than the estimates for other land cover types (1.40–3.20 g C kg^{-1} H_2O) and agreed well with measurements. For the wetland sites, the eWUE was slightly underestimated when compared to the measurements.

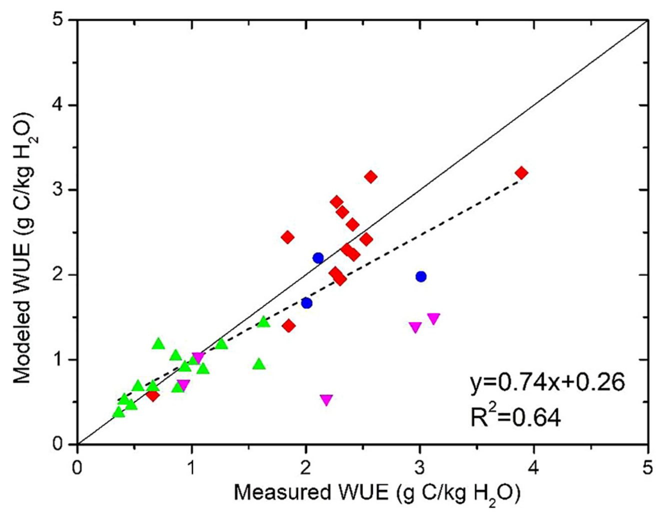

Fig. 3. The model-based eWUE vs. EC-based measurements. The solid and dashed lines are the 1:1 and regression lines, respectively. The triangle, inverted triangle, dot and inverted rectangle denote grasslands, croplands, wetlands and forests sites, respectively. The values of model-based eWUE were from grids that encompass the tower locations.

3.3. Spatial pattern of annual eWUE over China

Fig. 4 shows the spatial distributions of the mean annual DLM GPP, LSMs-ET and eWUE, and the standard deviation of annual eWUE for 1979–2012. Overall, the spatial pattern of the eWUE (Fig. 4c) was similar to GPP (Fig. 4a), but different from ET (Fig. 4b). Compared to the GPP and ET, the eWUE pattern also had a significantly larger spatial variability. The highest annual eWUE regions were found in the forest region in northeast China, where the annual GPP was relatively high, while ET was relatively low. It was consistent with the GPP pattern, in which all the forest regions in northeast, central, southwest and south China had a high eWUE. The cropland regions in north and northeast China had a relatively low eWUE and the north and Tibetan Plateau grassland areas had the lowest eWUE.

According to our eWUE estimates, the mean annual eWUE over China for 1979–2012 was 1.48 ± 1.04 g C kg^{-1} H_2O. ~9.4% of the vegetated land in China had an annual eWUE larger than 3.0 g C kg^{-1} H_2O, ~22.3% had an annual eWUE within the range of 2.0–3.0 g C kg^{-1} H_2O, ~28.4% had an annual eWUE from 1.0 to 2.0 g C kg^{-1} H_2O, and ~39.9% had an annual eWUE lower than 1.0 g C kg^{-1} H_2O.

Fig. 4d suggests that the standard deviation of annual eWUE ranged from 0.05 to 0.87 g C kg^{-1} H_2O. The regions with high eWUE in northeast, southwest, central and south China had higher standard deviations (> 0.1 g C kg^{-1} H_2O). In contrast, in the north and west China where there was a low eWUE, the standard deviations were smaller, and generally less than 0.1 g C kg^{-1} H_2O. The spatial distribution of the coefficient of variation of the annual eWUE (Fig. S3) clearly showed that the inter-annual variations in eWUE were relatively small in most areas of east and south China. In contrast, in some desert and surrounding regions in northwest China, the inter-annual variations in eWUE were high. The vegetation types in these regions were mainly shrublands and grasslands, where both GPP and ET were strongly influenced by the inter-annual variations in climatic factors, such as precipitation.

3.4. Spatio-temporal variations of annual eWUE over China

Fig. 5 shows the inter-annual variation of the spatially averaged eWUE over China from 1979 to 2012. An insignificant and positive trend, with a value of 7.32×10^{-4} g C kg^{-1} H_2O yr^{-1} was found,

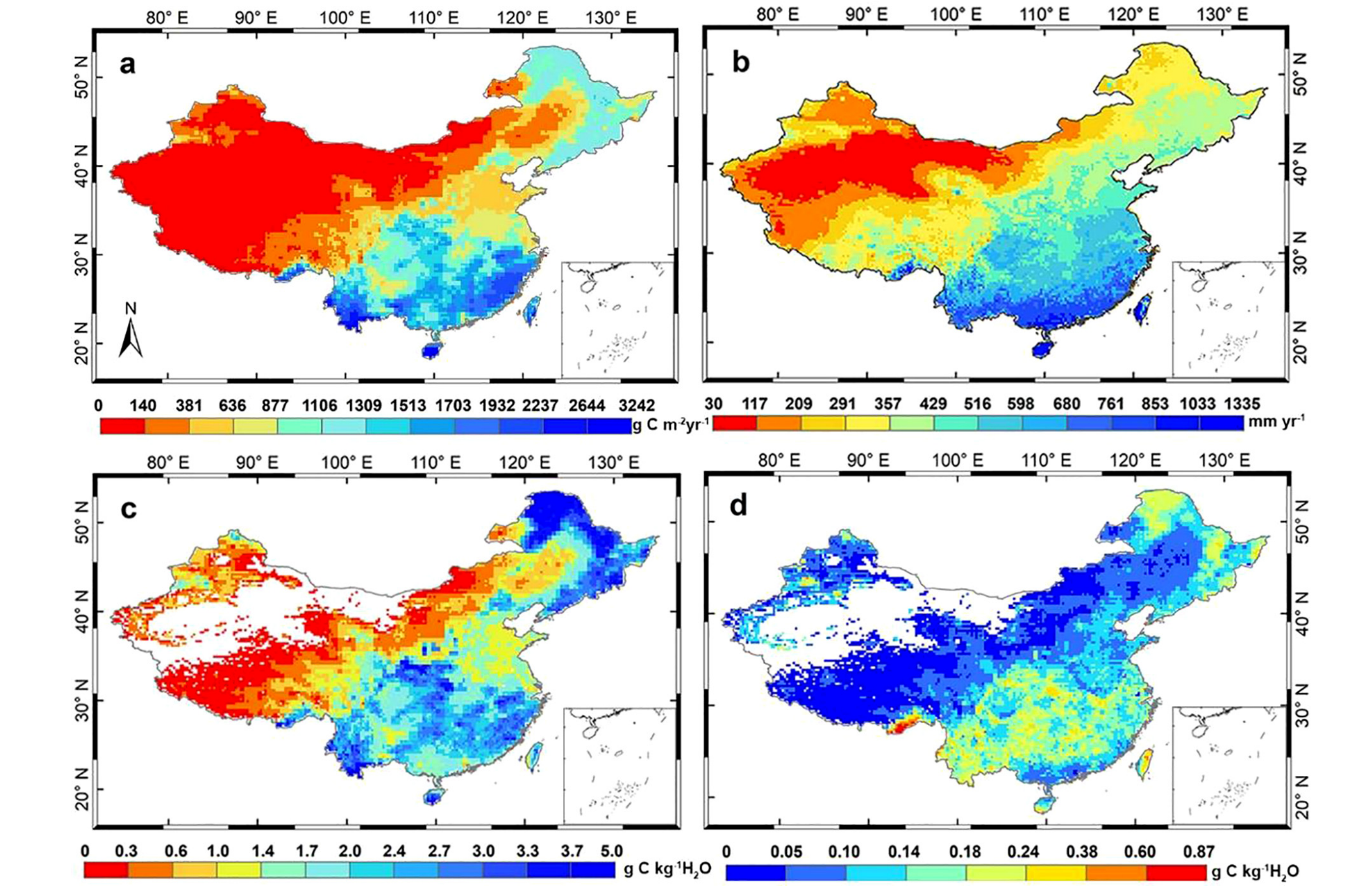

Fig. 4. The spatial distributions of the mean annual GPP, ET and eWUE, and the standard deviation of annual eWUE in China over 1979–2012. a. The mean annul GPP from the DLM simulations in this study; b. the mean annual ET of the LSMs-ET from Sun et al. (2017); c. the mean annual eWUE based on the DLM GPP and LSMs-ET datasets; d. the standard deviation of annual eWUE over 1979–2012.

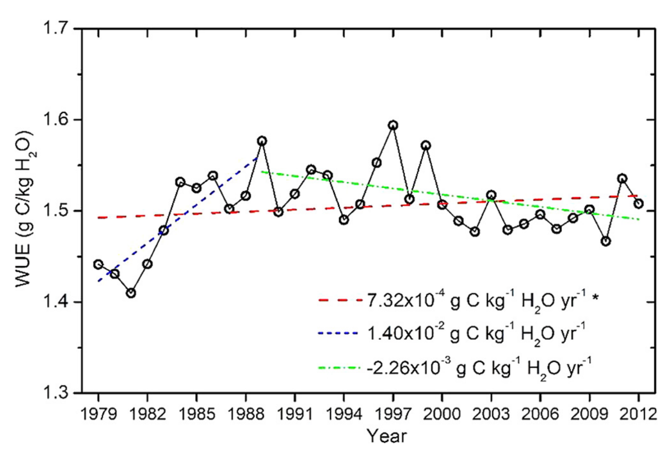

Fig. 5. Inter-annual variations of spatially averaged eWUE over China during 1979–2012. The dashed line is the regression line. * indicates that the trend is not significant ($p > 0.05$).

indicating that the annual eWUE in China slightly increased over the past three decades. A BP was detected in 1989, which divided the whole annual eWUE series into two periods, with significantly different eWUE trends. In the 1979–1989 period, the spatially averaged annual eWUE significantly increased at a rate of 1.40×10^{-2} g C kg^{-1} H_2O yr^{-1} ($p < 0.01$). In contrast, after 1989 it significantly decreased, with a value of -2.26×10^{-3} g C kg^{-1} H_2O yr^{-1} ($p < 0.01$).

The spatial distribution of M-K based annual eWUE changes showed that, ~21.4%, ~16.9%, and ~12.2% of the vegetated land in China experienced an increase ($p < 0.1$), medium increase ($p < 0.05$), and significant increase ($p < 0.01$) eWUE during 1979–2012, respectively (Fig. 6). These increased eWUE regions were dispersedly distributed in northeast, southwest and central China. In contrast, ~19.0%, ~15.2%, and ~11.3% of the vegetated land in China had a decrease ($p < 0.1$), medium decrease ($p < 0.05$), and significant decrease ($p < 0.01$) eWUE, respectively. These decreased eWUE regions were mainly found in deserts and their surrounding regions in west China and parts of northeast, southeast, and southwest China. In ~59.6% of the vegetated land in China the eWUE changes were insignificant, and mainly distributed in north China, east China and the south Tibetan Plateau.

Moreover, we calculated the mean annual eWUE of different vegetation function types and analyzed their inter-annual variations. The results showed that the DNF had the highest mean annual eWUE, followed by DBF, MF, EBF, SN, ENF, CL, GL and Shrub (Table 2). The DBF and ENF had significantly increasing eWUE trends ($p < 0.05$), with values of 3.0×10^{-3} and 3.1×10^{-3} g C kg^{-1} H_2O yr^{-1}, respectively. The EBF, MF, CL, GL and SN showed increasing trends, but the trends were not significant, with values of 1.2×10^{-4}, 2.2×10^{-3}, 1.5×10^{-3} 2.1×10^{-4} and 1.7×10^{-3} g C kg^{-1} H_2O yr^{-1}, respectively (Fig. 7). In contrast, the DNF and Shrub had insignificantly decreasing eWUE trends, with values of -4.8×10^{-3} and -5.0×10^{-4} g C kg^{-1} H_2O yr^{-1}, respectively. These results indicated that the slightly increasing eWUE over China during 1979–2012 (Fig. 5) was mainly resulted from the eWUE increases in forest, savannas and cropland vegetation types.

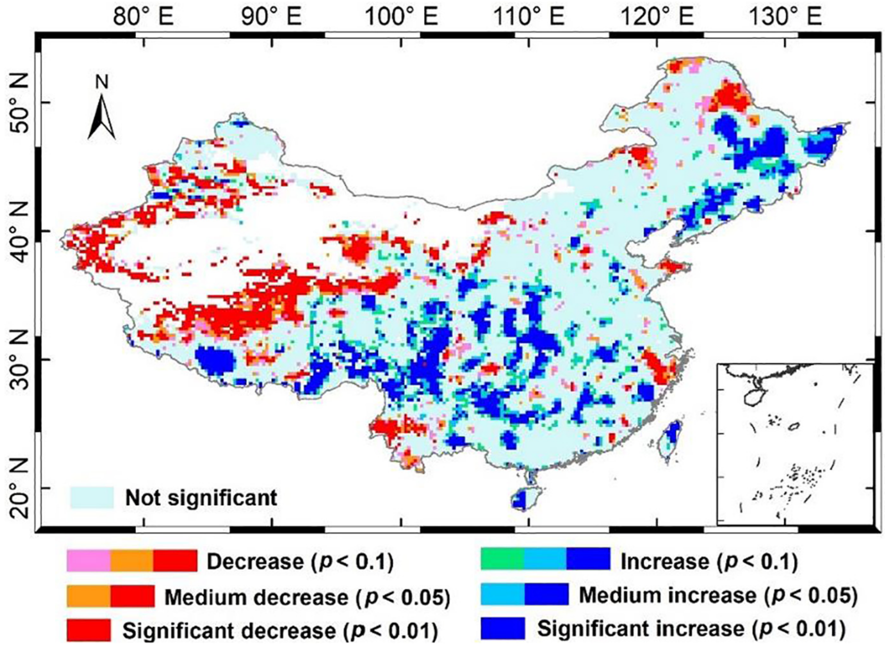

Fig. 6. The change levels of annual eWUE in China during 1979–2012. The levels were determined with the M-K test method.

Table 2
The mean annual eWUE of different vegetation function types in China over 1979–2012.

Vegetation function types	Mean annual WUE (g C kg^{-1} H_2O)
DBF	2.81 ± 0.07
DNF	3.82 ± 0.15
EBF	2.54 ± 0.11
ENF	2.27 ± 0.08
MF	2.69 ± 0.07
CL	1.76 ± 0.05
GL	0.86 ± 0.03
Shrub	0.79 ± 0.02
SN	2.31 ± 0.07

3.5. Effects of the inter-annual variations of AP, AMT and AMLAI on eWUE

Here, we examined the responses of inter-annual variations of eWUE to two climatic drivers (AP and AMT) and one biotic driver (AMLAI). First, we compared the detrended anomalies between spatially averaged annual eWUE and that of the drivers. The results showed that the inter-annual variations in AP, AMT, and AMLAI all had considerable effects on eWUE (Fig. 8). However, the magnitudes of the effects were significantly different. The AP seemed to have a dominant role in controlling year-to-year variation in eWUE during some periods (e.g., 1999–2007), but not in the other periods. There was no significantly identical variation between the eWUE and AMT anomalies. The year-to-year variation in spatially averaged AMLAI and eWUE was identical well during 1982–1989, but not for the other periods. These results indicated that the inter-annual variation of eWUE was largely determined by the combined effects of multiple drivers. We compared the spatial distribution of the trends of annual eWUE and that of the drivers (Fig. 9). The result showed that there was no a similar spatial pattern between the eWUE trend and the drivers' trends, further demonstrated the largely combined effects of multiple drivers on eWUE variation.

To quantify the responses of the inter-annual variations of eWUE to that of the each driver, we calculated the apparent sensitivities (i.e., the regression coefficients in Eq. (1)). Because the GIMMS3g LAI covers the period from 1982 to 2011, and a BP was detected in 1986 for the spatially averaged annual eWUE over 1982–2011, the regression coefficients were calculated for the whole eWUE period (1982–2011), significantly increasing eWUE period (1982–1986) and significantly decreasing eWUE period (1986–2011), respectively (Table 3). The results showed that except the AMT sensitivity in the decreasing eWUE period (δ_{tem}, −0.54), the other sensitivities were insignificant. Nevertheless, these sensitivities still reflected the relative contributions of the variations in each driver to eWUE. The inter-annual variation of eWUE was negatively correlated with AP, with sensitivities of −0.19, −0.27, and 0.13 for the whole eWUE period, increasing eWUE period, and decreasing eWUE period, respectively. The inter-annual variation of eWUE was also negatively correlated to AMT, but the sensitivities were much higher than that of AP, with values of −0.39, −2.39 and −0.54 for the whole, increasing and decreasing eWUE periods, respectively. In contrast, the responses of eWUE to AMLAI were positive, with sensitivities of 0.15, 0.56 and 0.03 for the whole, increasing and decreasing eWUE periods, respectively.

Fig. 10 shows the spatial distributions of the partial correlation coefficients between annual eWUE and the drivers, and spatial distribution of the eWUE dominant driver over China during 1982–2011. The inter-annual variation of eWUE was significantly correlated with AP in ~44.2% of vegetated land in China, in which ~98% was negative and mainly distributed in northeast China, Inner Mongolia and Tibetan Plateau areas. In ~16.2% of the vegetated land in China the inter-annual variation of eWUE was significantly correlated with AMT. ~76.9% and ~23.1% of these eWUE-AMT significantly correlated regions had negative and positive partial correlation values, respectively. The negatively correlated regions were dispersedly distributed in central, south and west China, and the positively correlated regions were mainly founded in some small areas in Tibetan Plateau. In contrast to AP and AMT, the inter-annual variation of AMLAI was significantly correlated with eWUE in only ~6.4% of vegetated land in China, which dispersedly distributed over China.

The eWUE dominant driver map was constructed by identified pixels with significant and maximum partial correlation values between eWUE and the drivers. It suggested that in ~41.4%, ~9.9% and ~3.1% of vegetated land in China the inter-annual variation of eWUE was dominated by variations in AP, AMT, and AMLAI, respectively. In Tibetan Plateau and north China AP was the most important driver, but

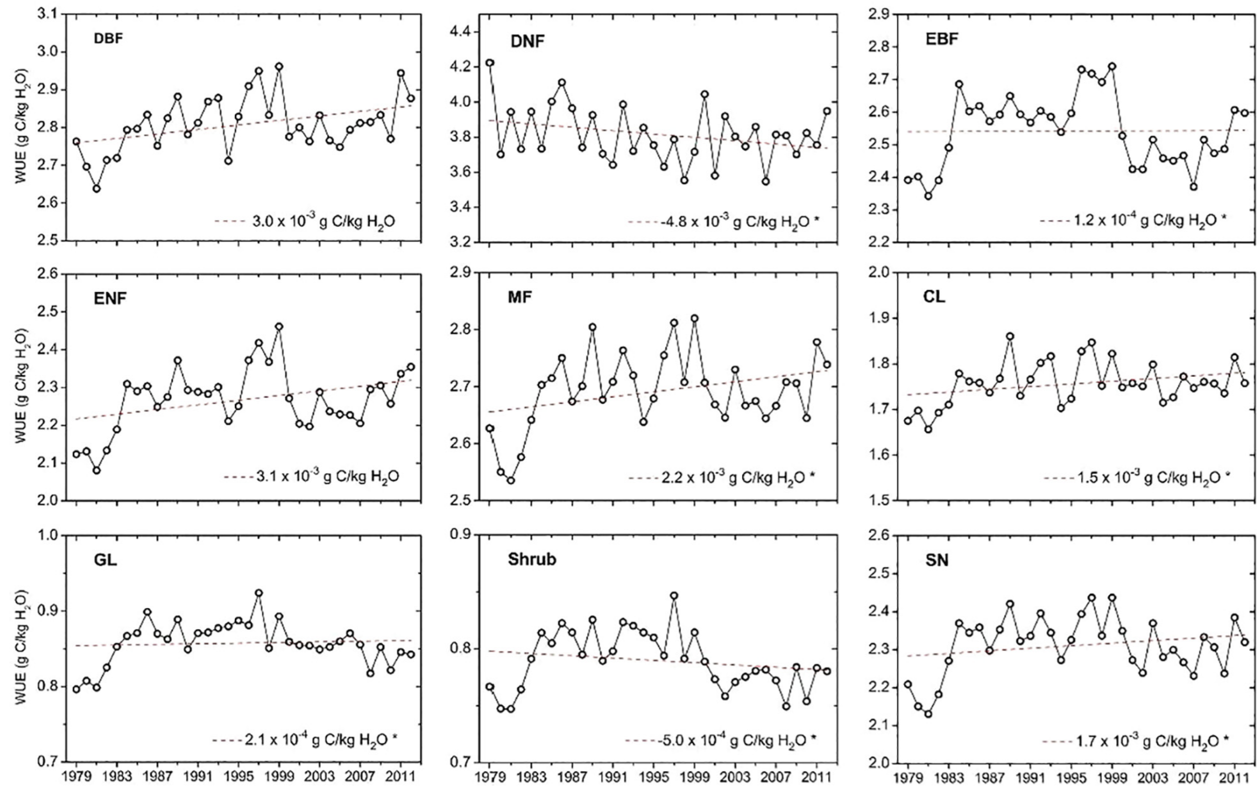

Fig. 7. The spatially averaged annual eWUE trends of different vegetation function types in China during 1979–2012. * indicates that the trend is not significant ($p > 0.05$).

in central, east and south China except AP, AMT, and AMLAI, inter-annual variations in the other factors (e.g., rising-CO_2, N deposition and solar radiation et. al.) that beyond the scope of this study also significantly contributed to the eWUE variation.

4. Discussion

4.1. The pattern and variations of annual eWUE in China

Unlike the patterns of GPP and ET, with their significantly latitudinal gradients, our eWUE estimates suggested that eWUE over China had a large spatial variability, with the highest eWUE in forest regions around 50°N, followed by a high eWUE in forest and savanna regions between 20 and 35°N, a low eWUE in croplands between 20 and 50°N, and the lowest eWUE in grasslands and shrublands between 28 and 50°N (Fig. 4c). These eWUE geographic characteristics agreed well with the eWUE latitudinal variations in the Northern Hemisphere as determined from FLUXNET sites (Tang et al., 2014) and independent process-based model simulations (Zhang et al., 2014; Liu et al., 2015). As reported by Tang et al. (2014), this latitude and vegetation type dependency in eWUE pattern means that eWUE is determined not only by several environmental or physiological variables, but also by the complicated effects of a multiplicity of abiotic and biotic factors.

When investigating the inter-annual variations of spatially averaged annual eWUE, we found an insignificant and positive annual eWUE trend in China during the last three decades, with a value of $7.32 \times 10^{-4}\,g\,C\,kg^{-1}\ H_2O\ yr^{-1}$. This positive trend was consistent with independent global eWUE trends reported by Cheng et al. (2017) and Huang et al. (2015). Using a newly developed eWUE model Cheng et al. (2017) reported a global eWUE trend of $13.7 \times 10^{-3}\,g\,C\,kg^{-1}$ $H_2O\ yr^{-1}$ ($p < 0.001$) during 1982–2012. Huang et al. (2015) found that global eWUE trend values were 1.0×10^{-4}, 7.0×10^{-4}, and $5.6 \times 10^{-3}\,g\,C\,kg^{-1}\ H_2O\ yr^{-1}$ during 1982–2008 for the nitrogen deposition, climate change and rising-CO_2 scenarios, respectively. By determining the BP of the annual eWUE series, we found that before 1989, eWUE significantly increased ($p < 0.01$), with a trend value of $1.4 \times 10^{-2}\,g\,C\,kg^{-1}\ H_2O\ yr^{-1}$, and significantly decreased ($p < 0.01$) at a rate of $-2.26 \times 10^{-3}\,g\,C\,kg^{-1}\ H_2O\ yr^{-1}$ after 1989. These changes in the eWUE trend were similar to that reported for Asia and global by Zhang et al. (2014) and Tang et al. (2014), respectively. Using process-based model eWUE estimate, Zhang et al. (2014) found that the annual eWUE did not substantially change in East Asia during 1982–2006, but had increasing and decreasing trends for the 1982–1995 and 1995–2006 periods, respectively. These eWUE trends were similar to our result in Fig. 5, and the small difference was caused by the different study period and area and uncertainties in the eWUE estimates. Based on the MODIS GPP and ET data, Tang et al. (2014) reported a negative global annual eWUE trend, with a value of $-4.5 \times 10^{-3}\,g\,C\,kg^{-1}\ H_2O\ yr^{-1}$ for the 2000–2013 period. Nevertheless, the inter-annual variations of eWUE from our study (Figs. 6 & 9a) were not quite consistent with that reported by Liu et al. (2015). A reasonable explanation was that the study periods in our study (1979–2012) and Liu et al. (2015) (2000–2011) was different. Besides, it also related with the uncertainties of the GPP estimates used in different studies.

In spatial distribution, we found that the significant eWUE changes areas over study period showed large spatial variability. The main reason was that eWUE is closely related with vegetation function types. As shown in Fig. 7, different vegetation types may have significant different trends, even though they existed under same climate condition (Fig. 1). Moreover, the large spatial variability in precipitation may be also an important reason (Fig. 9).

Overall, in many regions of northern, eastern, and southern China, the southern Tibetan Plateau and northern Xinjiang the annual eWUE over China did not significantly changed during the past three decades. On one hand, in some of these regions significant increases in precipitation enhanced vegetation growth (Fig. 9d), but with the increasing precipitation and temperature ET was also increased. As a

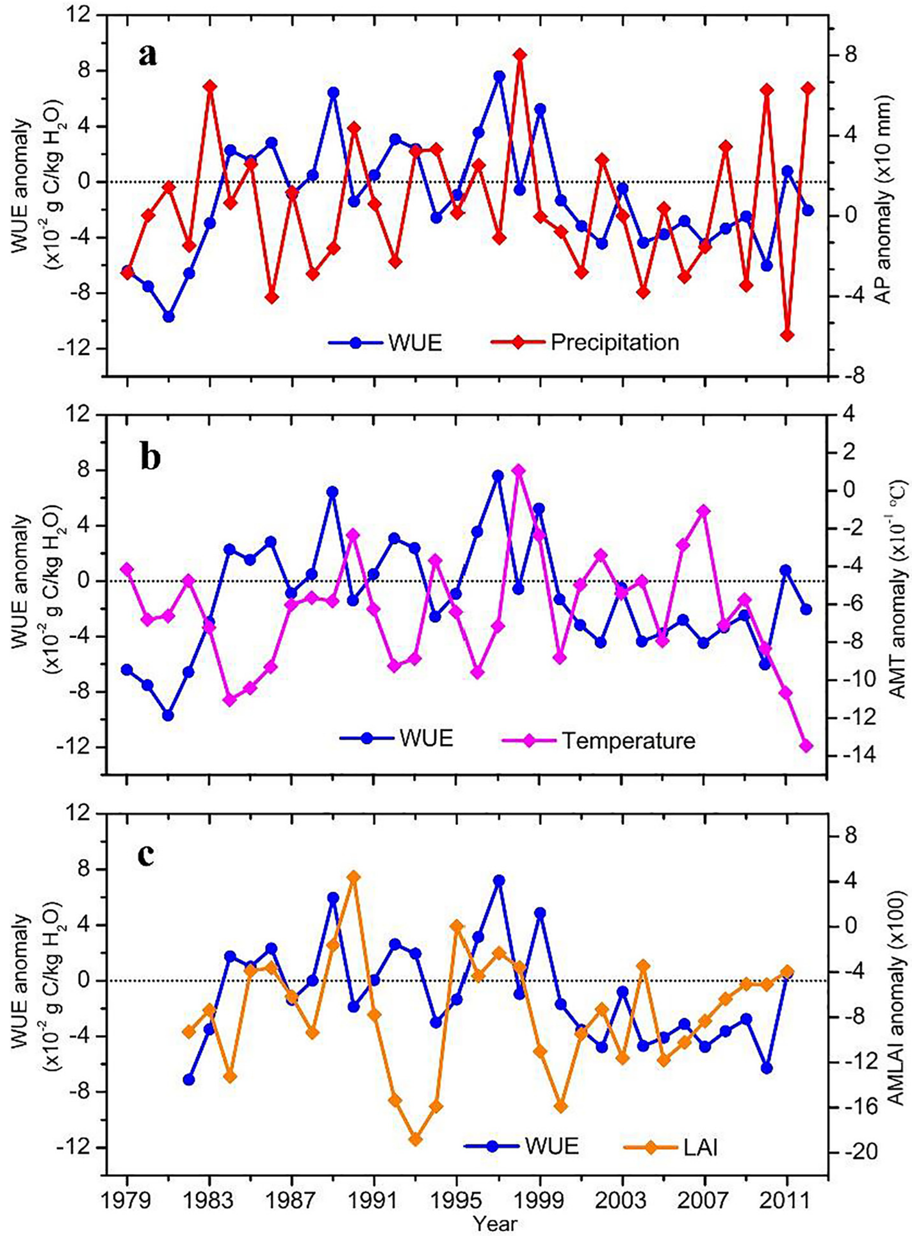

Fig. 8. Comparisons of the detrended anomalies of spatially averaged annual eWUE and its drivers over China.

result, changes in eWUE may be not significant (e.g., northern Xinjiang and north China). On the other hand, the spatial distributions of the trends of GPP (Fig. S4) and ET (Fig. S5) suggested that in many of these regions the small changes in both GPP and ET generated insignificant eWUE trends. The regions with significantly increasing eWUE were scattered over central, northeast and southwest China. In central and southwest China, although precipitation was decreasing in some areas, LAI and temperature were increasing, and resulted in increasing eWUE. A possible reason was that ET is energy-limited rather than water-limited in these regions. As Yu et al. (2008) reported, in the northeast China forest regions, both GPP and ET significantly increase with warming, and the increasing rate of GPP is faster. The significantly warming during the last three decades (Fig. 9c) generated increasing eWUE in northeast China. The regions with significantly decreasing eWUE were mostly distributed in the north Tibetan Plateau and desert regions in northwest China. In these regions, ET is water-limited and vegetation is sparse. Both the increases of precipitation and temperature (Fig. 9b and c) resulted in significantly increasing ET, but relative small changes in vegetation growth (Figs. S4 and S5). Thus, the eWUE was significantly decreasing in these arid regions.

4.2. The responses of eWUE variation to AP, AMT and AMLAI

Using our eWUE estimates, we examined the responses of the inter-annual variation of eWUE to precipitation, temperature, and LAI over China. We found that the inter-annual variation of the spatially averaged annual eWUE over China was negatively correlated with AP and AMT, and positively correlated with AMLAI. For the AP, it was consistent with previous EC-based results reported by Yu et al. (2008), but different with Xiao et al. (2013) and Zhu et al. (2015). Base on EC-derived eWUE from three forest sites, Yu et al. (2008) reported that annual eWUE linearly decreased with increasing AP. In comparison, using measurements from more EC sites, Xiao et al. (2013) and Zhu et al. (2015) found that annual eWUE changed with AP in a logarithmical manner. This discrepancy was because our analyses was based on integrated regional eWUE rather than site measurements. In addition,

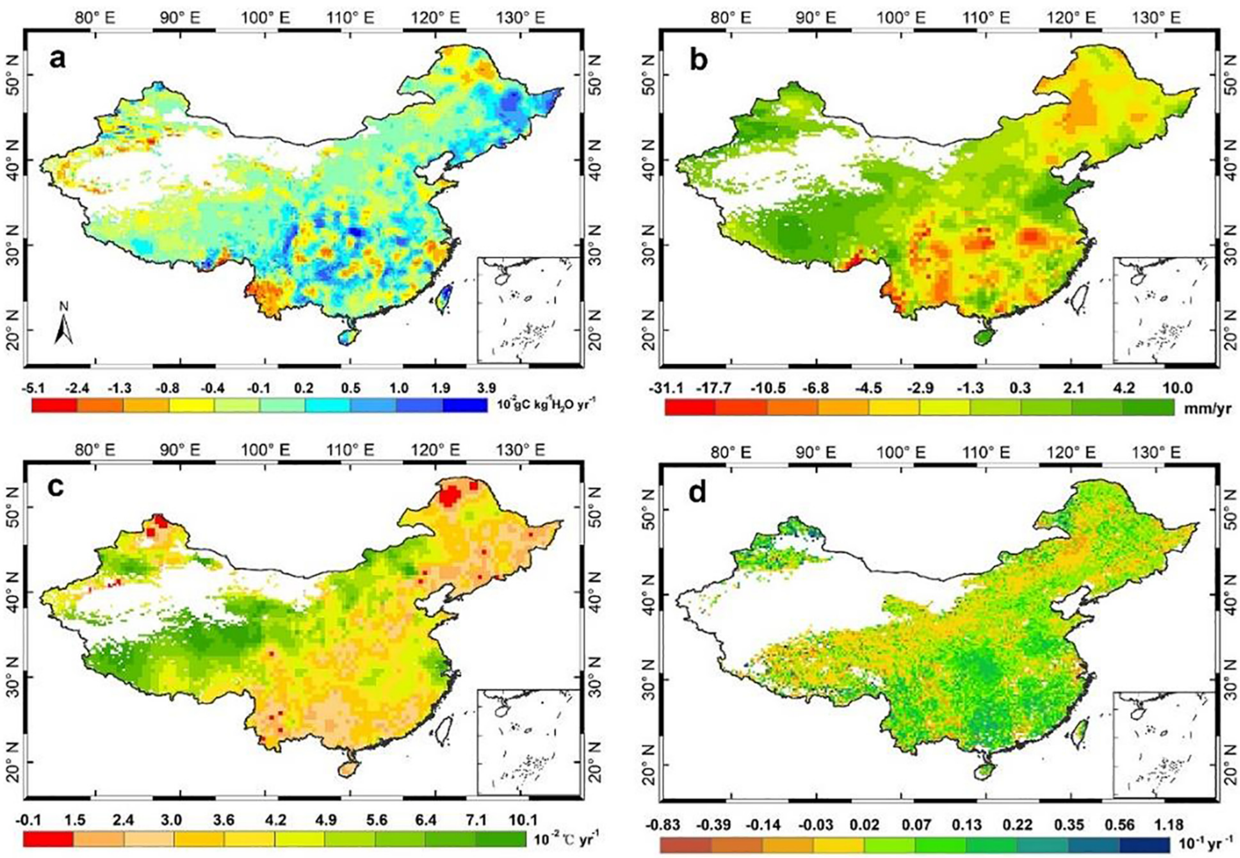

Fig. 9. Spatial distributions of the trends of eWUE (a), AP (b), AMT (c), and AMLAI (d) over China during 1982–2011.

Table 3
The trends of spatially averaged annual eWUE and the sensitivities of eWUE variation to its drivers over China.

Period[a]	WUE trend[b] (g C kg^{-1} H_2O yr^{-1})	Regression coefficients			
		γ_{pre}	δ_{tem}	φ_{lai}	*P*-value
1982–2011	$-6.47\times10^{-4*}$	−0.19 *	−0.39 *	0.15 *	0.26
1982–1986	2.40×10^{-2}	−0.27 *	−2.39 *	0.56 *	0.26
1986–2011	-1.84×10^{-3}	−0.13 *	−0.54	0.03 *	0.08

[a] A break point was detected in 1986.
[b] *Indicates insignificant ($p > 0.05$).

we found that the significant and negative eWUE-AP correlated regions covered most areas of northeast China, Inner Mongolia, and Tibetan Plateau. An explaination is in these arid and semi-arid regions when AP was increasing the rate of increase was faster for ET than GPP, and vice versa. In a recent experimental study, Zhang et al. (2015b) also confirmed this hypothesis. Through a manipulative experiment, Zhang et al. (2015b) found that in the semiarid temperate steppe of northern China, additional precipitation (i.e., over and above the natural precipitation) had a significantly positive effect on the ecosystem CO_2 exchange but had a trivial effect on GPP.

Based on EC-derived eWUE, Zhu et al. (2015) reported that there was a positive and linearly correlation between annual eWUE and MAT. In contrast, in this study we found that the spatially averaged annual eWUE over China was negatively correlated to MAT. Analogous to the eWUE-AP result, this difference might be duo to the annual eWUE used in our study was regionally integrated values rather than EC-based measurements at site scale. Besides, we compared the patterns of annual eWUE and MAT (Fig. S6) and found that the MAT for high eWUE regions (> 3.0 g C kg^{-1} H_2O) ranged from −5 °C in northeast China to 20 °C in southwest China. This result further demonstrated that there were no a significant linear relationship between eWUE and MAT at large scales and across a range of ecosystems.

Previous EC-based and process-based model eWUE studies have showed that LAI strongly affected eWUE and even primarily determined the eWUE seasonal and inter-annual variations (Hu et al., 2008; Zhang et al., 2014). For example, based on model experiments (scenario analysis), Zhang et al. (2014) conclude that the increases in eWUE over East Asia during 1982–2006 were firstly attributed to the increased LAI, followed by the effects of meteorological factors. In contrast, our sensitivity analyses showed that although the spatially averaged annual eWUE was positively correlated with AMLAI, the regions with significant eWUE-AMLAI correlation were only found in 6.4% of the vegetated land in China. This limited effect of AMLAI on eWUE mainly because of the non-linear relationship between eWUE and AMLAI. As reported by Liu et al. (2015), and Tong et al. (2009), although annual eWUE rapidly increased with increasing AMLAI when AMLAI was less than ∼1.5 (depending on vegetation types), it slowly increased even decreased with increases in AMLAI under large AMLAI. The patterns of AMLAI (Fig. S7) over China showed that except the AP and AMT dominant regions (Fig. 10d) AMLAI values in the other regions were larger than 1.5.

4.3. Uncertainties in the GPP and eWUE datasets

We validated our DLM GPP estimate against the EC-derived GPP from 16 flux towers and compared it with two independent GPP datasets (MTE and MODIS). Our GPP estimate performed better than the MTE and MODIS GPPs at the site scale, and had a similar spatial pattern to the MODIS and MTE GPPs at the regional scale. However, uncertainties still inevitably remained in our GPP estimate. First, as with the MODIS and MTE GPP, the DLM model underestimated cropland

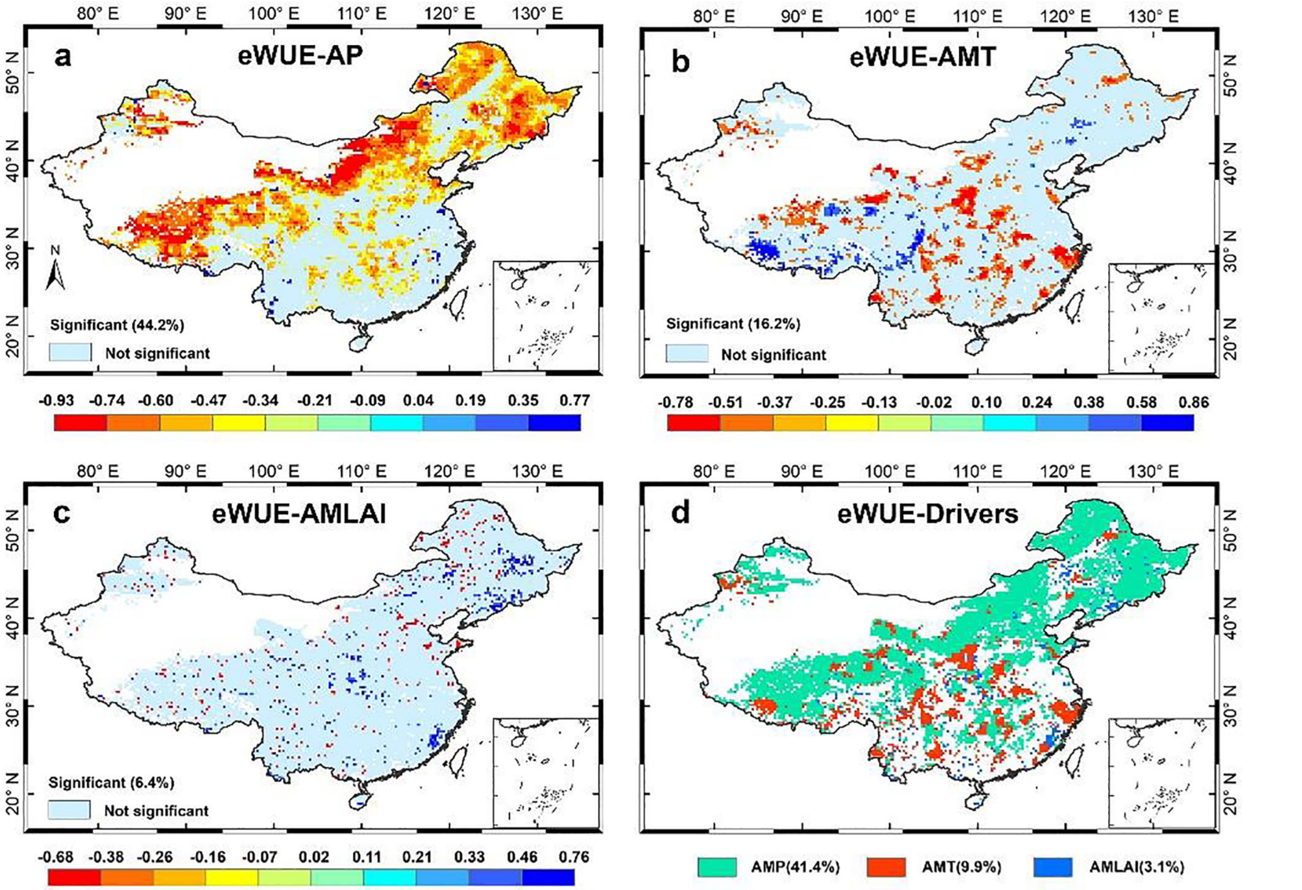

Fig. 10. Spatial distributions of the partial correlation coefficients between eWUE and AP (a), AMT (b), and AMLAI (c), and spatial distribution of eWUE dominant driver during 1982–2011 over China (d).

GPP, indicating that the model parameterizations for cropland should be further improved. Second, our DLM GPP had a similar pattern to the other independent GPP products, but with a lower mean annual GPP (5.66 Pg C) when compared with some of them. For example, the MTE-based GPP from Jung et al. (2011) (MTE-Jung, 6.52 Pg C) and Yao et al. (2017) (MTE-Yao, 6.62 Pg C), and EC-LUE GPP (6.04 Pg C) from Li et al. (2013) had a higher mean annual GPP. These differences might have resulted from the underestimation of DLM GPP for cropland, and might also be due to the differences in the time periods of the different datasets: DLM (1979–2012), MTE-Jung (1982–2011), MTE-Yao (1982–2015) and EC-LUE (2000–2009). Nevertheless, it should also be noticed that the mean annual value of our DLM GPP was higher than that of MODIS (5.16 Pg C) and EC-LUE GPP (5.38 Pg C) from Yuan et al. (2010).

We validated our eWUE estimates against EC-derived eWUE from 35 flux towers. Overall, our eWUE estimates agreed well with EC-based eWUE. Not surprisingly, eWUE was underestimated for some cropland sites, because of the underestimation in GPP estimates at these sites. There were also several limitations in our EC-based site validations, which also resulted in uncertainties. The first limitation was the scale issue. Our modeled and EC-derived eWUE represented spatial scales of $0.25^{\circ} \times 0.25^{\circ}$ (~25 km) and 1–3 km, respectively. This scale mismatch may arise considerable uncertainties for the validations. The second limitation was the uncertainties from the EC-based eWUE, which was derived as the ratio of EC-based GPP to ET. The NEE partitioning GPP method results in significant uncertainties in EC-GPP (Rawlins et al., 2015) and the energy closure issues of EC measurements result in uncertainties in both EC-derived GPP and ET (Hjhendricks et al., 2011). As a result, these EC-based GPP and ET uncertainties induce the EC-eWUE uncertainties, which may also significantly affect the evaluations of our eWUE estimates.

5. Conclusion

In this study, using GPP and ET simulations from process-based models, we estimated the eWUE in China during 1979–2012, quantified its spatio-temporal pattern and examined the effects of the inter-annual variations in AP, MAT, and AMLAI on it. The main findings are as follows:

(1) Except for a few cropland sites the DLM-based eWUE estimates agreed well with EC-derived values. The large uncertainties of eWUE estimates in cropland sites were mainly due to the significant underestimations in the DLM modelled GPP at those sites, suggesting that the photosynthesis parameterizations of cropland in the model should be further refined.
(2) The spatially averaged annual eWUE over China was $1.48 \pm 1.04\,\mathrm{g\,C\,kg^{-1}\,H_2O}$, and had a slightly increasing but not significant trend ($7.32\times10^{-4}\,\mathrm{g\,C\,kg^{-1}\,H_2O\,yr^{-1}}$, $p < 0.05$) from 1979 to 2012. The spatial distribution of the eWUE trend showed large spatial variability. ~21.4% and ~19.0% of vegetated land in China had significant increasing and decreasing trends ($p < 0.1$), respectively. The increasing eWUE was mainly found in northeast, southwest and central of China, while the decreasing eWUE was mostly distributed in west China and parts of northeast, southeast, and southwest China.
(3) The inter-annual variation of spatially averaged eWUE over China was negatively correlated with that of AP and AMT, but positively correlated with that of AMLAI. In ~41.4%, ~9.9% and ~3.1% vegetated land of China the inter-annual variation of eWUE was

dominated by AP, AMT, and AMLAI, respectively. In most land of north China and west China, AP was the dominant drivers. In central China, east China, and south China, except the AP, AMT, and AMLAI dominated the eWUE inter-annual variation in some regions the other factors (ring-CO_2, drought, N deposition, and solar radiation, et. al.) that did not involve in this study also played dominant role.

Overall, our eWUE estimates and analyses provided valuable datasets and information for understanding the carbon-water coupling mechanisms of terrestrial ecosystem. Nevertheless, the other environmental factors, such as, the ring-CO_2, drought, N deposition, and radiation that also have impacts on eWUE variations were not considered in this study. Future studies should further explore the effects of these factors on eWUE.

Acknowledgments

The authors thank the Data Assimilation and Modeling Center for Tibetan Multi-spheres, ITP-CAS for providing the model forcing datasets, the Land-Atmosphere Interaction Research Group at Beijing Normal University for providing the model soil texture inputs and Liu et al. (2015) for their previous China EC-WUE data work. The authors also thank Dr. Jing Chen and Dr. Guang Xu for their help on model calibrating and the GIMMS3g data processing. This work was supported the by National Natural Science Foundation of China (41522207, 41571130042, 41271116, 41881114); and the State's Key Project of Research and Development Plan of China (2016YFA0601002).

References

Beer, C., Ciais, P., Reichstein, M., Baldocchi, D., Law, B.E., Papale, D., et al., 2009. Temporal and among-site variability of inherent water use efficiency at the ecosystem level. Global Biogeochem. Cycles 23, GB2018.
Boese, S., Jung, M., Carvalhais, N., Reichstein, M., 2017. The importance of radiation for semiempirical water-use efficiency models. Biogeosciences 14, 3015–3026.
Bruemmer, C., Black, T.A., Jassal, R.S., Grant, N.J., Spittlehouse, D.L., Chen, B., et al., 2012. How climate and vegetation type influence evapotranspiration and water use efficiency in Canadian forest, peatland and grassland ecosystems. Agric. Forest Meteorol. 153, 14–30.
Chen, B., Che, M., 2016. Improving vegetation phenological parameterization of a land surface model. Biogeosci. Discuss. 1–59. http://dx.doi.org/10.5194/bg-2016-165.
Chen, B., Chen, J.M., Mo, G., Yuen, C.-W., Margolis, H., Higuchi, K., et al., 2007a. Modeling and scaling coupled energy, water, and carbon fluxes based on remote sensing: an application to Canada's landmass. J. Hydrometeorol. 8, 123–143.
Chen, B., Chen, J.M., Ju, W., 2007b. Remote sensing-based ecosystem-atmosphere simulation scheme (EASS)-Model formulation and test with multiple-year data. Ecol. Model. 209, 277–300.
Chen, B., Xu, G., Coops, N.C., Ciais, P., Innes, J.L., Wang, G., et al., 2014. Changes in vegetation photosynthetic activity trends across the Asia-Pacific region over the last three decades. Remote Sens. Environ. 144, 28–41.
Chen, J., Chen, B., Black, T.A., Innes, J.L., Wang, G., Kiely, G., et al., 2013. Comparison of terrestrial evapotranspiration estimates using the mass transfer and Penman-Monteith equations in land surface models. J. Geophys. Res.-Biogeo. 118, 1715–1731.
Cheng, L., Zhang, L., Wang, Y.P., Canadell, J.G., Chiew, F.H.S., Beringer, J., et al., 2017. Recent increases in terrestrial carbon uptake at little cost to the water cycle. Nat. Commun. 8, 110.
Friedl, M.A., McIver, D.K., Hodges, J.C., Zhang, X., Muchoney, D., Strahler, A.H., et al., 2002. Global land cover mapping from MODIS: algorithms and early results. Remote Sens. Environ. 83, 287–302.
Gang, C., Wang, Z., Chen, Y., Yang, Y., Li, J., Cheng, J., et al., 2016. Drought-induced dynamics of carbon and water use efficiency of global grasslands from 2000 to 2011. Ecol. Ind. 67, 788–797.
Guanter, L., Zhang, Y., Jung, M., Joiner, J., Voigt, M., Berry, J.A., et al., 2014. Global and time-resolved monitoring of crop photosynthesis with chlorophyll fluorescence. Proc. Natl. Acad. Sci. USA 111, E1327–E1333.
Guerrieri, R., Lepine, L., Asbjornsen, H., Xiao, J., Ollinger, S.V., 2016. Evapotranspiration and water use efficiency in relation to climate and canopy nitrogen in US forests. J. Geophys. Res.-Biogeo. 121, 2610–2629.
Helman, D., Osem, Y., Yakir, D., Lensky, I.M., 2017. Relationships between climate, topography, water use and productivity in two key Mediterranean forest types with different water-use strategies. Agric. Forest Meteorol. 232, 319–330.
Hjhendricks, F., Stöckli, R., Lehner, I., Rotenberg, E., Seneviratne, S.I., 2011. Energy balance closure of eddy-covariance data: a multisite analysis for European FLUXNET stations. Agric. Forest Meteorol. 150, 1553–1567.
Hu, Z., Yu, G., Fu, Y., Sun, X., Li, Y., Shi, P., et al., 2008. Effects of vegetation control on ecosystem water use efficiency within and among four grassland ecosystems in China. Global Change Biol. 14, 1609–1619.
Huang, L., He, B., Han, L., Liu, J., Wang, H., Chen, Z., 2017. A global examination of the response of ecosystem water-use efficiency to drought based on MODIS data. Sci. Total Environ. 601–602, 1097–1107.
Huang, M., Piao, S., Sun, Y., Ciais, P., Cheng, L., Mao, J., Wang, Y., 2015. Change in terrestrial ecosystem water-use efficiency over the last three decades. Global Change Biol. 21, 2366–2378.
Huang, M., Piao, S., Zeng, Z., Peng, S., Ciais, P., Cheng, L., et al., 2016. Seasonal responses of terrestrial ecosystem water-use efficiency to climate change. Global Change Biol. 22, 2165–2177.
Ito, A., Inatomi, M., 2012. Water-use efficiency of the terrestrial biosphere: a model analysis focusing on interactions between the global carbon and water cycles. J. Hydrometeorol. 13, 681–694.
Jones, H., Black, T.A., Jassal, R.S., Nesic, Z., Grant, N., Bhatti, J.S., Sidders, D., 2017. Water balance, surface conductance and water use efficiency of two young hybrid-poplar plantations in Canada's aspen parkland. Agric. Forest Meteorol. 246, 256–271.
Jung, M., Reichstein, M., Margolis, H.A., Cescatti, A., Richardson, A.D., Arain, M.A., et al., 2011. Global patterns of land-atmosphere fluxes of carbon dioxide, latent heat, and sensible heat derived from eddy covariance, satellite, and meteorological observations. J. Geophys. Res.-Biogeo. 116 (G3).
Keenan, T.F., Hollinger, D.Y., Bohrer, G., Dragoni, D., Munger, J.W., Schmid, H.P., Richardson, A.D., 2013. Increase in forest water-use efficiency as atmospheric carbon dioxide concentrations rise. Nature 499, 324–327.
Kendall, M., 1975. Rank Correlation Methods. Griffin, London.
Knauer, J., Zaehle, S., Reichstein, M., Medlyn, B.E., Forkel, M., Hagemann, S., Werner, C., 2017. The response of ecosystem water-use efficiency to rising atmospheric CO_2 concentrations: sensitivity and large-scale biogeochemical implications. New Phytol. 213, 1654–1666.
Li, X., Liang, S., Yu, G., Yuan, W., Cheng, X., Xia, J., et al., 2013. Estimation of gross primary production over the terrestrial ecosystems in China. Ecol. Model. 261–262, 80–92.
Liu, L., Hu, C., Olesen, J.E., Ju, Z., Zhang, X., 2016. Effect of warming and nitrogen addition on evapotranspiration and water use efficiency in a wheat-soybean/fallow rotation from 2010 to 2014. Climatic Change 139, 565–578.
Liu, Q., Ma, M., Wang, W., Huang, G., Zhang, Z., Tan, J., 2008. WATER: Dataset of eddy covariance observations at the Yingke oasis station. Cold and Arid Regions Environmental and Engineering Research Institute Chinese Academy of Sciences.
Liu, S., Xu, Z., Zhu, Z., Jia, Z., Zhu, M., 2013. Measurements of evapotranspiration from eddy-covariance systems and large aperture scintillometers in the Hai River Basin. China. J. Hydrol. 487, 24–38.
Liu, Y., Xiao, J., Ju, W., Zhou, Y., Wang, S., Wu, X., 2015. Water use efficiency of China's terrestrial ecosystems and responses to drought. Sci. Rep. 5, 13799.
Lu, X., Zhuang, Q., 2010. Evaluating evapotranspiration and water-use efficiency of terrestrial ecosystems in the conterminous United States using MODIS and AmeriFlux data. Remote Sens. Environ. 114, 1924–1939.
Ma, M., Wang, W., Jin, R., Huang, G., Zhang, Z., Tan, J., 2008. WATER: Dataset of eddy covariance observations at the A'rou freeze/thaw observation station. Cold and Arid Regions Environmental and Engineering Research Institute Chinese Academy of Sciences.
Mann, H.B., 1945. Nonparametric tests against trend. Econometrica 13, 245–259.
Mu, Q., Heinsch, F.A., Zhao, M., Running, S.W., 2007. Development of a global evapotranspiration algorithm based on MODIS and global meteorology data. Remote Sens. Environ. 111, 519–536.
Oleson, K.W., Lawrence, D.M., Gordon, B., Flanner, M.G., Kluzek, E., Peter, J., et al., 2010. Technical description of version 4.0 of the Community Land Model (CLM). NCAR Technical Note NCAR/TN-478 + STR. National Center for Atmospheric Research, Boulder.
Oliveira, D., Brunsell, G.N.A., Moraes, E.C., Shimabukuro, Y.E., Bertani, G., Santos, T.V., Aragao, L.E.O.C., 2017. Evaluation of MODIS-based estimates of water-use efficiency in Amazonia. Int. J. Remote Sens. 38, 5291–5309.
Piao, S., Sitch, S., Ciais, P., Friedlingstein, P., Peylin, P., Wang, X., et al., 2013. Evaluation of terrestrial carbon cycle models for their response to climate variability and to CO_2 trends. Global Change Biol. 19, 2117–2132.
Ponton, S., Flanagan, L.B., Alstad, K.P., Johnson, B.G., Morgenstern, K.A.I., Kljun, N., et al., 2006. Comparison of ecosystem water-use efficiency among Douglas-fir forest, aspen forest and grassland using eddy covariance and carbon isotope techniques. Global Change Biol. 12, 294–310.
Quan, Q., Zhang, F., Tian, D., Zhou, Q., Wang, L., Niu, S., 2018. Transpiration dominates ecosystem water-use efficiency in response to warming in an alpine meadow. J. Geophys. Res.-Biogeo. 123. http://dx.doi.org/10.1002/2017JG004362.
Rawlins, M.A., McGuire, A.D., Kimball, J.S., Dass, P., Lawrence, D., Burke, E., et al., 2015. Assessment of model estimates of land-atmosphere CO_2 exchange across Northern Eurasia. Biogeosciences 12, 4385–4405.
Reichstein, M., Ciais, P., Papale, D., Valentini, R., Running, S., Viovy, N., et al., 2007. Reduction of ecosystem productivity and respiration during the European summer 2003 climate anomaly: a joint flux tower, remote sensing and modelling analysis. Global Change Biol. 13, 634–651.
Shangguan, W., Dai, Y., Liu, B., Zhu, A., Duan, Q., Wu, L., et al., 2013. A China data set of soil properties for land surface modeling. J. Adv. Model. Earth Sy. 5, 212–224.
Sun, S., Chen, B., Ge, M., Qu, J., Che, T., Zhang, H., et al., 2016a. Improving soil organic carbon parameterization of land surface model for cold regions in the Northeastern Tibetan Plateau, China. Ecol. Model. 330, 1–15.
Sun, S., Chen, B., Shao, Q., Chen, J., Liu, J., Zhang, X.-J., et al., 2017. Modeling evapotranspiration over China's landmass from 1979 to 2012 using multiple land surface

models: evaluations and analyses. J. Hydrometeorol. 18, 1185–1203.
Sun, Y., Piao, S., Huang, M., Ciais, P., Zeng, Z., Cheng, L., et al., 2016b. Global patterns and climate drivers of water-use efficiency in terrestrial ecosystems deduced from satellite-based datasets and carbon cycle models. Global Ecol. Biogeogr. 25, 311–323.
Tang, X., Li, H., Desai, A.R., Nagy, Z., Luo, J., Kolb, T.E., et al., 2014. How is water-use efficiency of terrestrial ecosystems distributed and changing on Earth? Sci. Rep. 4, 7483.
Tang, X., Ma, M., Ding, Z., Xu, X., Yao, L., Huang, X., et al., 2017. Remotely monitoring ecosystem water use efficiency of grassland and cropland in China's arid and semi-arid regions with MODIS data. Remote Sens. 9, 616.
Tian, H., Lu, C., Chen, G., Xu, X., Liu, M., Ren, W., et al., 2011. Climate and land use controls over terrestrial water use efficiency in monsoon Asia. Ecohydrology 4, 322–340.
Tong, X.-J., Li, J., Yu, Q., Qin, Z., 2009. Ecosystem water use efficiency in an irrigated cropland in the North China Plain. J. Hydrol. 374, 329–337.
Tucker, C.J., Pinzon, J.E., Brown, M.E., Slayback, D.A., Pak, E.W., Mahoney, R., et al., 2005. An extended AVHRR 8-km NDVI dataset compatible with MODIS and SPOT vegetation NDVI data. Int. J. Remote Sens. 26, 4485–4498.
Wang, J., Bai, J., Chen, X., Luo, G., Wang, S., 2015. Carbon fluxes in cotton field with plastic mulched drip irrigation in Xinjiang Oasis. Trans. Chin. Soc. Agr. Mach 46, 70–78.
Wang, X., Wang, T., Liu, D., Guo, H., Huang, H., Zhao, Y., 2017. Moisture-induced greening of the South Asia over the past three decades. Global Change Biol. 23, 4995–5005.
Wang, Z., Xiao, X., Yan, X., 2010. Modeling gross primary production of maize cropland and degraded grassland in northeastern China. Agric. Forest Meteorol. 150, 1160–1167.
Xiao, J., Sun, G., Chen, J., Chen, H., Chen, S., Dong, G., et al., 2013. Carbon fluxes, evapotranspiration, and water use efficiency of terrestrial ecosystems in China. Agric. Forest Meteorol. 182, 76–90.
Xie, J., Chen, J., Sun, G., Zha, T., Yang, B., Chu, H., et al., 2016. Ten-year variability in ecosystem water use efficiency in an oak-dominated temperate forest under a warming climate. Agric. Forest Meteorol. 218–219, 209–217.
Xue, B.-L., Guo, Q., Otto, A., Xiao, J., Tao, S., Li, L., 2015. Global patterns, trends, and drivers of water use efficiency from 2000 to 2013. Ecosphere 6, 174.
Yan, J.W., Liu, J., Chen, B., Feng, M., Fang, S.F., Xu, G., et al., 2014. Changes in the land surface energy budget in eastern China over the past three decades: contributions of land-cover change and climate change. J. Climate 27, 9233–9252.
Yang, K., He, J., Tang, W., Qin, J., Cheng, C.C., 2010. On downward shortwave and longwave radiations over high altitude regions: observation and modeling in the Tibetan Plateau. Agric. Forest Meteorol. 150, 38–46.
Yao, Y., Wang, X., Li, Y., Wang, T., Shen, M., Du, M., et al., 2017. Spatiotemporal pattern of gross primary productivity and its covariation with climate in China over the last thirty years. Global Change Biol. 24, 184–196.
Yu, G., Song, X., Wang, Q., Liu, Y., Guan, D., Yan, J., et al., 2008. Water-use efficiency of forest ecosystems in eastern China and its relations to climatic variables. The New phytol. 177, 927–937.
Yu, G.-R., Wen, X.-F., Sun, X.-M., Tanner, B.D., Lee, X., Chen, J.-Y., 2006. Overview of ChinaFLUX and evaluation of its eddy covariance measurement. Agric. Forest Meteorol. 137, 125–137.
Yu, Z., Wang, J., Liu, S., Rentch, J.S., Sun, P., Lu, C., 2017. Global gross primary productivity and water use efficiency changes under drought stress. Environ. Res. Lett. 12, 014016.
Yuan, W., Liu, S., Yu, G., Bonnefond, J., Chen, J., Davis, K., et al., 2010. Global estimates of evapotranspiration and gross primary production based on MODIS and global meteorology data. Remote Sens. Environ. 114, 1416–1431.
Zhang, F., Ju, W., Shen, S., Wang, S., Yu, G., Han, S., 2014. How recent climate change influences water use efficiency in East Asia. Theor. Appl. Climatol. 116, 359–370.
Zhang, L., Ge, H., 2014. Gross primary production in Phyllostachys edulis based on MODIS. J. Zhejiang Agr. Forest Univ. 31, 178–184.
Zhang, L., Tian, J., He, H., Ren, X., Sun, X., Yu, G., et al., 2015a. Evaluation of water use efficiency derived from MODIS products against eddy variance measurements in China. Remote Sens. 7, 11183–11201.
Zhang, X., Tan, Y., Li, A., Ren, T., Chen, S., Wang, L., Huang, J., 2015b. Water and nitrogen availability co-control ecosystem CO_2 exchange in a semiarid temperate steppe. Sci. Rep. 5, 15549.
Zhang, Y., Song, C., Sun, G., Band, L.E., Mcnulty, S., Noormets, A., et al., 2016. Development of a coupled carbon and water model for estimating global gross primary productivity and evapotranspiration based on eddy flux and remote sensing data. Agric. Forest Meteorol. 223, 116–131.
Zhao, M., Running, S.W., 2010. Drought-induced reduction in global terrestrial net primary production from 2000 through 2009. Science 329, 940–943.
Zhou, S., Yu, B., Huang, Y., Wang, G., 2014. The effect of vapor pressure deficit on water use efficiency at the subdaily time scale. Geophys. Res. Lett. 41, 5005–5013.
Zhu, X.-J., Yu, G., Wang, Q., Hu, Z., Zheng, H., Li, S., et al., 2015. Spatial variability of water use efficiency in China's terrestrial ecosystems. Global Planet. Change 129, 37–44.
Zhu, Z., Bi, J., Pan, Y., Ganguly, S., Anav, A., Xu, L., et al., 2013. Global data sets of vegetation leaf area index (LAI) 3g and fraction of photosynthetically active radiation (FPAR)3g derived from global inventory modeling and mapping studies (GIMMS) normalized difference vegetation index (NDVI3g) for the period 1981 to 2011. Remote Sens. 5, 927–948.